European Cells and Materials Vol.47 2024 (pages 73–90) DOI: 10.22203/eCM.v047a06 ISSN 1473-2262

Original Article

A NOVEL MOUSE MODEL OF POLYTRAUMA WITH SPINAL CORD INJURY–ASSOCIATED HETEROTOPIC OSSIFICATION

R. Aita[1], G. Unnithan[2], T. Klaylat[1,3], J.A. Petruccelli[1], G. St-Jean[4], M. Radhakrishna[2], R. Gawri[1,3] and C. Gao[1,2,*]

[1]Department of Surgery, McGill University, Montréal, QC H3A 1A4, Canada
[2]Department of Medicine, McGill University, Montréal, QC H3A 1A4, Canada
[3]Division of Orthopaedic Surgery, Department of Surgery, Regenerative Orthopaedics and Innovation Laboratory, McGill University, Montréal, QC H3A 1A4, Canada
[4]Department of Pathology and Microbiology, Faculty of Veterinary Medicine, Université de Montréal, Saint-Hyacinthe, QC J2S 2M2, Canada

Abstract

Heterotopic ossification (HO) refers to abnormal bone formation in soft tissues, which is a common complication of traumatic spinal cord injury (SCI). Current therapeutic approaches are non-specific, have limited efficacy and pose serious off-target effects due to insufficient knowledge of HO mechanisms. In the absence of clinically relevant models of traumatic SCI-associated HO, a novel mouse model of polytrauma with concomitant SCI and musculotendinous injury (MTI) was developed. SCI was induced by T9-T10 spinal cord transection, and muscle crush/tenotomy was performed on left quadricepses (SCI+MTI), leaving right limbs intact as internal controls. Age and sex-matched control mice underwent left hindlimb MTI alone or SCI with left quadriceps crush only (SCI+MI). High-resolution micro-computed tomography revealed variable amounts of ectopic mineral deposits only in injured hindlimbs of SCI+MI and SCI+MTI mice. Median ectopic mineral volumes in SCI+MTI mice were higher than SCI+MI mice at 1 and 4 weeks postoperative. Histology of serial sections confirmed von Kossa-positive mineral colocalizing with ALP-positive osteoblast activity and TRAP-positive osteoclast activity, with a significant increase in ALP between both timepoints. Immunofluorescence indicated F4/80-positive macrophages infiltrating ectopic mineral in SCI+MTI mice at 1 week postoperative, and Osterix-positive osteoblasts lining trabecular bone in HO at 4 weeks postoperative. Orthotopic bone loss manifested as cortical thinning and trabecular bone loss in femurs of SCI mice at 4 weeks postoperative. This study thus identifies SCI+MTI mice as a clinically relevant small animal model of polytrauma with SCI in which to study pathogenic mechanisms and assess novel therapeutic approaches to SCI-associated HO.

Keywords: Polytrauma, spinal cord injury, musculotendinous injury, ectopic mineral, heterotopic bone, osteopenia.

***Address for correspondence**: Chan Gao, 1650 Cedar Ave, L7.510, Montreal, QC, H3G 1A3, Canada. Telephone number: (514) 934-1934 ext. 44185; Fax: (514) 934-8265; E-mail: chan.gao@mcgill.ca

Introduction

Heterotopic ossification (HO) is defined as abnormal bone formation in soft tissues like muscle and tendon. A high incidence of ectopic bone formation is associated with traumatic soft tissue injury during joint arthroplasty (Łęgosz *et al*., 2019), off-label use of bone morphogenetic protein (BMP) in spinal fusion (Weldon *et al*., 2023), extensive burn injuries (Agarwal *et al*., 2017b), and heritable defects in BMP signaling (Towler and Shore, 2022). Neurogenic HO refers to a specific form of traumatic HO arising from damage to the central nervous system (CNS) and peripheral nerves, which is reported in up to 50 % of individuals who have sustained polytrauma involving spinal cord injury (SCI) (Yolcu *et al*., 2020). In the case of traumatic SCI, predisposing factors to HO include complete SCI, spasticity, pressure sores, and secondary injuries arising from motor and sensory deficits (Banovac *et al*., 2004; Meyers *et al*., 2019; van Kuijk *et al*., 2002). SCI-associated HO commonly affects the muscles and tendons around hip and knee joints, causing pain and stiffness, which compromise rehabilitation and contribute to poor quality of life (van Kuijk *et al*., 2002). In the absence of sufficient knowledge regarding the etiology and pathogenesis of HO, non-specific treatments like radiation therapy, anti-inflammatory drugs, and bisphosphonates have limited prophylactic or therapeutic efficacy (Ampadiotaki *et al*., 2021). Furthermore, complete surgical resection of ectopic bone is challenging due to the propensity for damage to entrapped nerves and blood

vessels (Genêt *et al*., 2019).

The 2022 annual report of the National Spinal Cord Injury Statistic Center (NSCISC) reported traumatic SCI is attributed to vehicle crashes (37.6 %), falls (31.5 %), violence (15.4 %) and sports-related incidents (8.3 %) (uab.edu/NSCISC). Traumatic SCI sustained during these events is frequently accompanied by musculoskeletal injuries. Radiological and intraoperative findings consistently reveal the frequent involvement of both muscle and tendon in the neurogenic HO around hip, suggesting the occurrence of musculotendinous injuries (Arduini *et al*., 2015; Denormandie *et al*., 2018). Young adult C57Bl/6 mice with T10 spinal contusion injury and BMP2-infused hydrogel injected into the quadriceps muscle were used to model combat-related HO (Kang *et al*., 2014). A similar approach using T7-T8 or T11-T13 spinal cord transection and intramuscular cardiotoxin injection into the hamstring muscle was used to model SCI-associated traumatic HO (Genêt *et al*., 2015). Others have used a mouse model of traumatic brain injury (TBI) with intramuscular cardiotoxin to demonstrate intraperitoneal injection of the endogenous mineralization inhibitor pyrophosphate effectively inhibited cardiotoxin induced HO in skeletal muscle (Tőkési *et al*., 2020). Cardiotoxin has emerged as a useful tool in the study of muscle regeneration due to its ability to damage myocytes while sparing innervation, vascularization, and tendon (Wang *et al*., 2022). This stands in contrast to traumatic injuries, wherein all these vital components are often compromised. Furthermore, it was found that the healing trajectory and cellular activity varied significantly based on the mechanism of injury (Hardy *et al*., 2016), which should therefore be chosen carefully to ensure the clinical relevance of the animal models. Although these models identified an essential role for simultaneous CNS and peripheral tissue injury for the induction of neurogenic HO, they do not reflect the most frequent aetiologies.

Muscles and tendons around big joints like the hip, knee, and shoulder have been implicated in development of neurogenic HO (Meyers *et al*., 2019). To investigate the relative contributions of traumatic SCI and concomitant peripheral musculotendinous injuries to HO, three mouse models were developed: SCI with quadriceps muscle injury (SCI+MI), quadriceps musculotendinous injury (MTI) alone, and SCI+MTI. For each mouse the left hindlimb was injured and the right hindlimb left intact as an internal control. Therefore, a reproducible and clinically relevant mouse model of polytrauma involving SCI with concomitant MTI was developed. Quantitative micro-CT analyses, histochemical and immunofluorescence staining of cellular activity were used to characterise HO development in the injured quadriceps muscle of SCI+MTI mice.

Methods

Animal Care

All mouse procedures were approved for use by the Facility Animal Care Committee of McGill University (AUP 2021-8214) in accordance with the policies and guidelines of the Canadian Council on Animal Care (CCAC). Three-month-old female C57Bl/6 mice (The Jackson Laboratory, Bar Harbor, ME, USA) were acclimatized for one week under a 12-hour light/dark cycle with free access to food and water at the animal vivarium of the Research Institute of the McGill University Health Centre (RI-MUHC, Montreal General Hospital location). The experimental approach and random group allocation are outlined in Fig. 1. To eliminate confounding factors associated with the randomization of individual mice, the intact right hindlimb acted as Control for the injured left limb in MTI mice and as SCI alone in SCI+MTI mice.

Survival Surgery

General anesthesia was induced with 3 % isoflurane before placing mice in the prone position to make a 3 mm skin incision over the thoracic spine and dissect superficial dorsal muscles to expose the T9-T10 vertebral column (Fig. 1**a**). After stabilization of adjacent vertebrae, laminectomy and complete spinal cord transection (SCI) were performed before closing the wound. A 3 mm skin incision was then made on the lateral aspect of the left knee to expose the quadriceps tendon and patella to perform the hindlimb injury (Fig. 1**b**). A surgical clamp was used to apply a compressive force for 15 seconds to the musculotendinous junction to induce MI whereas MTI was achieved by sharp transection of the quadriceps tendon following MI.

Postoperative Care and Tissue Harvest

Mice were housed individually postoperative for the duration of the experiment. Pain relief was achieved by subcutaneous administration of 1mg/kg of buprenorphine SR three hours preoperative and every three days postoperative throughout the experiment. Soft food and water were placed in Petri dishes on the cage floor to permit easy access and adequate nutrition for paraplegic mice and their bladders were expressed manually twice daily. To ensure adequate tissue hydration all mice received 0.5 mL subcutaneous saline immediately after surgery and twice daily thereafter for one week. Cohorts of mice were euthanized at 1 or 4 weeks postoperative using isoflurane and CO_2 inhalation followed by cervical dislocation. The hindlimbs were isolated by transection of the femur and tibia while preserving the quadriceps muscle and its insertion at the patella. The samples were then fixed at 4 °C in 4 % paraformaldehyde overnight, rinsed in phosphate-buffered saline (PBS) pH 7.4 three times and stored at 4 °C in PBS until the time of analysis (Gao *et al*., 2013).

Micro-Computed Tomography (Micro-CT)

Fixed specimens were scanned on a Bruker Skyscan 1172 Micro-CT (Bruker, Kontich, Belgium) at a spatial resolution of 7 µm with a 0.5 mm aluminum filter, voltage of 50 kV and current of 200 µA as described previously (Lacourt *et al*., 2012). NRecon software version 1.0 (Bruker, Kontich, Belgium) was used for reconstruction with a setting of 4 for ring artifacts, 20 % beam hardening reduction and 0 smoothing. A dedicated algorithm in CTAn version 1.13 (Bruker, Kontich, Belgium) was used to analyze a region of interest (ROI) encircling only heterotopic mineral and bone spanning 4.2 mm, which was expressed as ectopic mineral volume (μm^3). The threshold used to define bone was $\geq$ 1335 Hounsfield units. Cortical and intramedullary trabecular bone were analyzed in the ROI of the distal femur and expressed as cross-sectional cortical bone area (Cort. B. Ar., 10^5 μm^2) and trabecular bone volume/tissue volume (Tra. BV/TV, %). Bone mineral density (g/cm^3) of cortical and trabecular bone of the distal femurs was calculated using Bruker-MicroCT BMD phantoms with calcium hydroxyapatite concentrations of 0.25 and 0.75 g/cm^3 (Körmendi *et al*., 2021).

Histochemical Staining and Quantitative Analyses

After micro-CT imaging, 6/11 SCI+MTI samples at 1 week and 6/13 SCI+MTI samples at 4 weeks postoperative were dehydrated using graded alcohol, embedded at low temperature in methyl methacrylate resin (MMA), and sectioned at 5 µm for histochemical staining as described previously (Gao *et al.*, 2012). Consecutive sections were stained with Von Kossa/Toluidine Blue (VK/TB) to distinguish mineralized from un-mineralized tissue (Valverde-Franco *et al*., 2004), Tartrate-Resistant Acid Phosphatase (TRAP) and Fast Green counterstain to identify osteolytic cells (Behrends *et al.*, 2014). Alkaline Phosphatase (ALP) in osteogenic cells was stained with a commercial kit according to the manufacturer's instructions (DISCOVERY ChromoMap Blue kit, CAT05266661001, Ventana) using Nuclear Fast Red as a counterstain.

Quantitative Histological Analysis

Sections at the mid-sagittal plane of each HO lesion were used for histochemical staining and quantitative analysis. The analytical approach integrating micro-CT and histological data was developed and described in previous publications (Gao *et al*., 2013; Lacourt *et al*., 2012). The mid-sagittal plane of HO lesions was identified on micro-CT images using Dataviewer software version 1.0 (Bruker, Kontich, Belgium) and used as a template for the identification of the corresponding position on MMA-embedded tissue. Quantitative analyses of % stained area on ALP and TRAP sections were performed blindly and independently by two lab members with an interrater variability of $<$ 20 % using the same $\times$20 magnification images and ImageJ analytical software version 1.53 (https://imagej.net/).

Immunohistochemistry

Immunofluorescence was performed on paraffin embedded tissue sections rehydrated in a graded series of ethanol and tap water followed by heat-induced epitope recovery using Citrate buffer. Then sections were treated with 3 % H_2O_2 for 10 min to inactivate endogenous peroxidase activity. Sections were blocked for 2 hours with 10 % normal goat serum and then incubated with primary antisera -Sp7/osterix 1:100 (ab22552, Abcam, Cambridge, MA) or F4/80 antiserum 1:50 (ab300421, Abcam, Cambridge, MA). Negative control sections were incubated with normal goat serum. After overnight incubation at 4 °C the sections were rinsed with PBS and incubated with Goat anti-rabbit IgG Alexa Fluor 488 1:500 (A11008, Invitrogen, Carlsbad, CA, USA) for 90 min at room temperature. Nuclei were counterstained for 10 min with DAPI 1 µg/mL (D3571, ThermoFisher Scientific, Hillsboro, OR, USA).

Statistical Analysis

Power analysis of preliminary data determined the number of animals required for each surgical intervention. A total of 60 mice were used for this study: SCI+MI = 17 mice, MTI = 12 mice and SCI+MTI = 31 mice. Two blinded evaluators validated the data from micro-CT and histological analysis of skeletal tissues. Statistical analysis was performed using GraphPad Prism software version 8.0.1 (GraphPad Software, Inc., San Diego, CA, USA). Data are expressed as median and interquartile range (IQR), with significance set at $p < 0.05$. Shapiro-Wilk test was used to assess whether datasets were normally distributed. Kruskal-Wallis test was used for non-parametric, unpaired comparisons of HO volume, Cort. B. Ar., Tra. BV/TV, Cort. BMD, and Tra. BMD among three or more groups at postoperative 1 and 4 weeks whereas Dunn's test was employed for post hoc analysis. Mann-Whitney U test was performed to compare quantification of ALP and TRAP staining between postoperative 1 and 4 weeks.

Results

The primary objective of this study was to characterize ectopic bone formation in a novel mouse model of traumatic SCI with MTI that was developed to mimic the complex injuries often sustained by adults in traffic accidents or falls. A secondary objective was to characterize changes in orthotopic bone over time in paralyzed SCI+MTI mice.

Shown in Fig. 1, the overall experimental design with the numbers of mice undergoing surgical procedures, subsequent exclusion criteria and numbers used for postmortem analyses are summarized. Postmortem analyses were performed on 7 SCI+MI, 6 MTI and 11 SCI+MTI mice at 1 week postoperative and 9 SCI+MI, 5 MTI and 13 SCI+MTI mice at 4 weeks postoperative. One mouse with SCI+MI was euthanized in the first week postoperative due to wound dehiscence (n = 1). Four mice with SCI+MTI were euthanized in the first week postoperative due to ex-

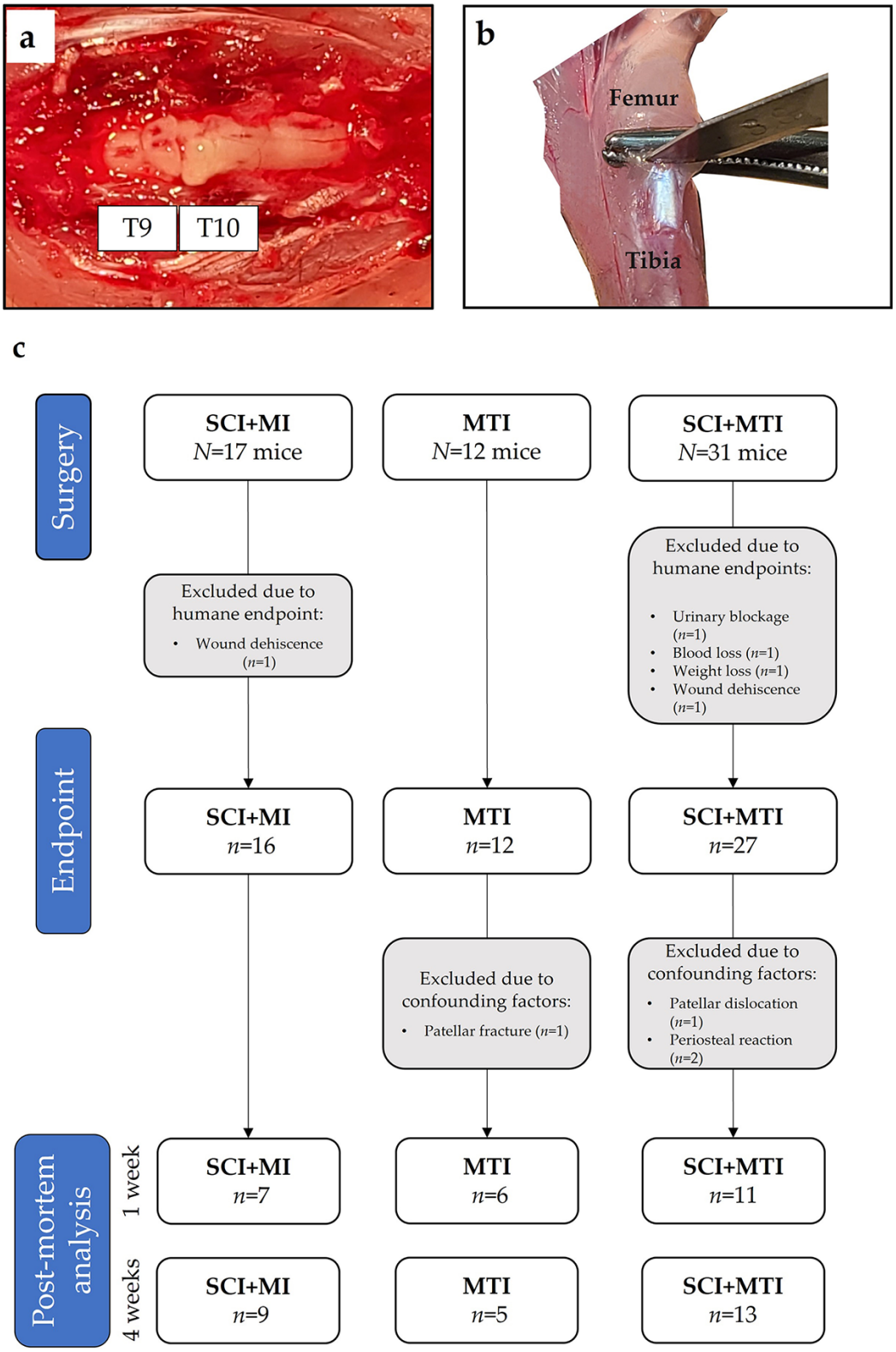

Fig. 1. Animal surgery and study design. Spinal cord injury (SCI) was induced by transection of the thoracic cord at T9-T10 (**a**). A surgical clamp was used to apply a compressive force for 15 seconds to the left quadriceps muscle at its junction with the quadriceps tendon to induce muscle injury (MI). In the case of musculotendinous injury (MTI) the quadriceps tendon was sharply transected following MI (**b**). The intact right quadriceps was used as an internal control. Mice were euthanized at 1 week or 4 weeks postoperative and the hindlimbs were harvested for radiologic imaging and histological analyses as illustrated in panel (**c**).

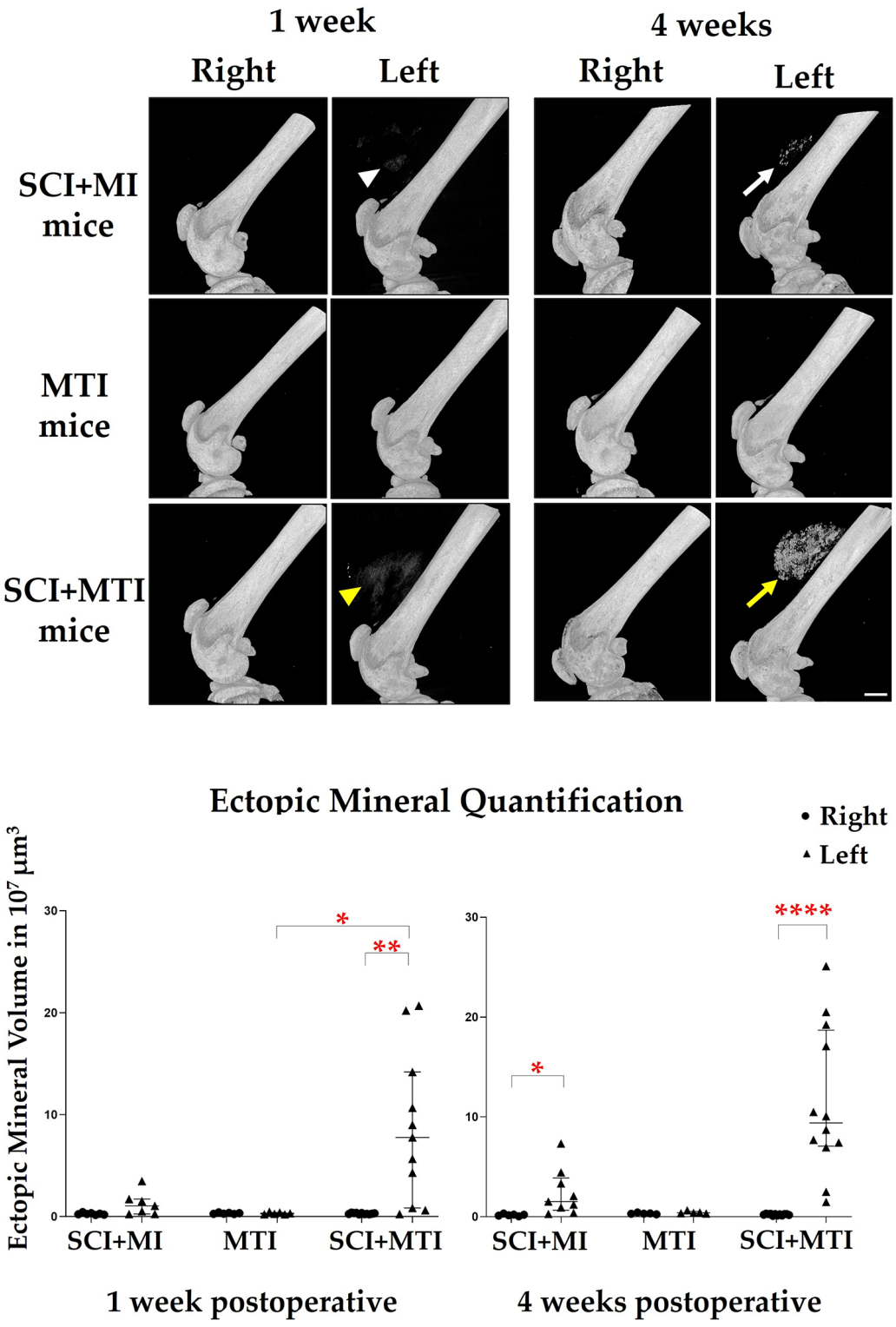

Fig. 2. Micro-CT analysis of SCI-associated ectopic mineral deposition and bone formation. Representative 3D-reconstructions of micro-CT images of the right (intact) and left (injured hindlimbs of SCI+MI, MTI alone or SCI+MTI mice were compared. At 1 week postoperative, diffuse ectopic mineral was seen at the site of quadriceps injury in the left hindlimb of SCI+MI mice (white arrowhead) with significantly more in SCI+MTI (yellow arrowhead). By 4 weeks postoperative there was a modest increase in diffuse mineral in SCI+MI mice (white arrow) while large deposits of ectopic bone (yellow arrow) had developed in the injured left hindlimb of SCI+MTI mice. Scale bar represents 1 mm. Quantitative analyses confirmed no ectopic mineral in the intact right limbs of any mice. The small volume seen in the left limb of SCI+MI mice at 1 week postoperative was significantly greater at 4 weeks postoperative ($p < 0.01$) compared to the right limb. p *<0.05, **<0.01, ****<0.0001.

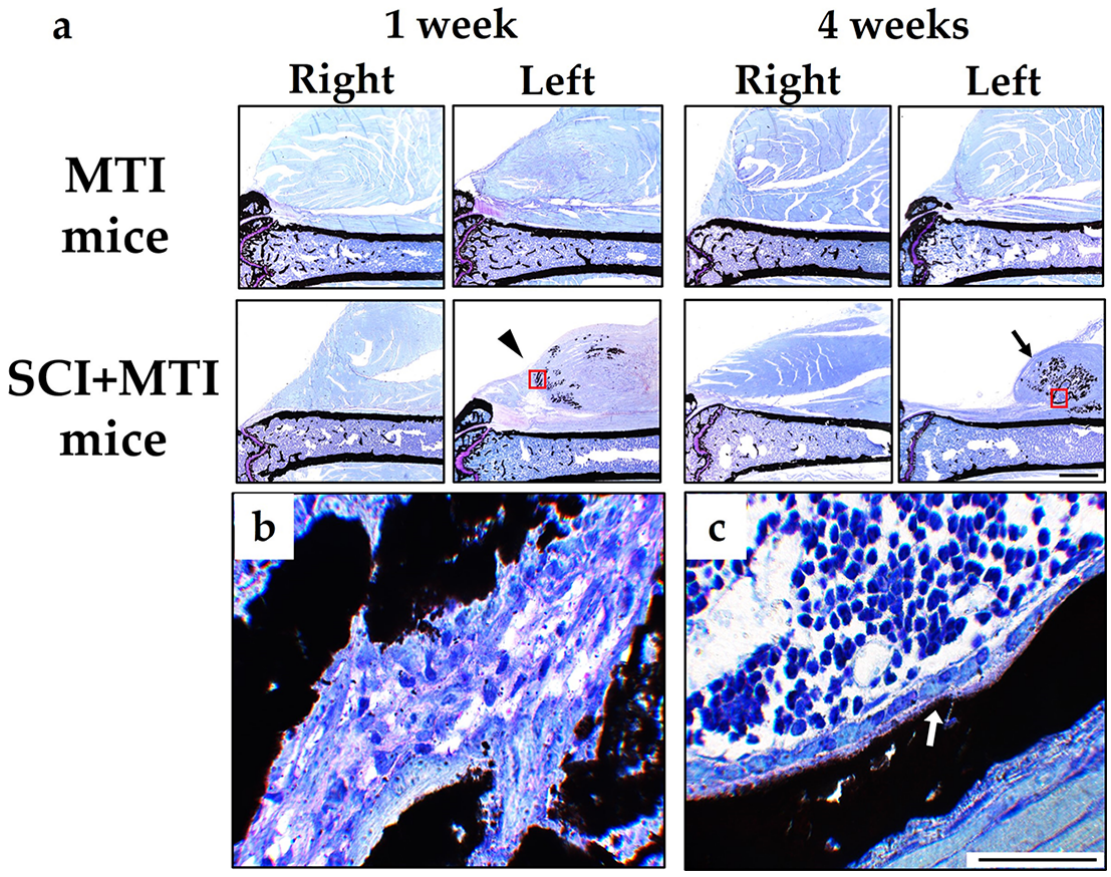

Fig. 3. Histologic analysis of SCI-associated ectopic mineral deposition and bone formation. Representative Von Kossa/Toluidine Blue stained sections of the distal femur (**a**) show diffuse mineral (arrowhead) deposited in the injured left quadriceps at 1 week and trabecular bone (arrow) at 4 weeks postoperative in SCI+MTI mice. Scale bar represents 1000 μm. High magnification images of the red insets in SCI+MTI mice show mineral with no trabecular structure surrounding condensed mesenchyme at 1 week (**b**) and trabeculae with cuboidal cells resembling osteoblasts surrounding marrow (**c**, white arrow) at 4 weeks postoperative. Scale bar represents 50 μm.

cessive blood loss (n = 1), urinary blockage (n = 1), significant weight loss (n = 1) and wound dehiscence (n = 1). Three additional mice were excluded from analysis due to patellar dislocation (n = 1) and periosteal reaction (n = 2). Only one mouse was excluded from the MTI Control group due to a patellar fracture.

In Fig. 2, the upper panels show representative 3D micro-CT reconstructions of the distal femora of surgically modified mice euthanized at 1 week and 4 weeks postoperative. Ectopic mineral deposition was visible as a radiopaque lesion adjacent to the femoral diaphysis above the patella in the injured left hindlimb of 4/7 SCI+MI (white arrowhead) and 10/11 SCI+MTI (yellow arrowhead) mice at 1 week postoperative. By 4 weeks postoperative the lesion covered approximately the same area but had assumed the radiologic appearance of trabecular bone in 7/9 SCI+MI (white arrow) and 13/13 SCI+MTI mice (yellow arrow). There was no evidence of ectopic mineral at any time in the left limbs of mice with MTI alone or in the uninjured right hindlimbs of any mice. Grubb's test detected one outlier in the SCI+MTI cohort at 4 weeks postoperative leading to a sample size of n = 12 for statistical analysis. Quantitative analysis of the volume of ectopic mineral deposited in the right and left quadriceps muscles confirmed the qualitative micro-CT data. The ectopic mineral volume in the left hindlimbs of SCI+MTI mice increased from a median of 7.8×10^7 μm^3 (IQR: 9.84) at 1 week to 9.4×10^7 μm^3 (IQR: 10.32) at 4 weeks postoperative. Since only SCI+MTI mice consistently demonstrated significantly higher amount of HO at 1 and 4 weeks postoperative in comparison to SCI alone, further characterization using histological analysis was focused on the mice with SCI+MTI.

Shown in Fig. 3, representative histologic sections of undecalcified hindlimbs with intact quadriceps were stained with Von Kossa and counterstained with Toluidine Blue (VK/TB) for structural analysis and mineral (black) content of orthotopic and heterotopic bone. Low magnification images (Fig. 3**a**) confirm the absence of mineral deposition in quadriceps muscle of MTI mice and an increase in heterotopic mineral from 1 week (arrowhead) to 4 weeks (arrow) postoperative in the injured left limbs of SCI+MTI. Higher magnification images of the tissue within the red insets of SCI+MTI mice reveal amorphous mineral deposits and condensed mesenchyme at 1 week postoperative (Fig.

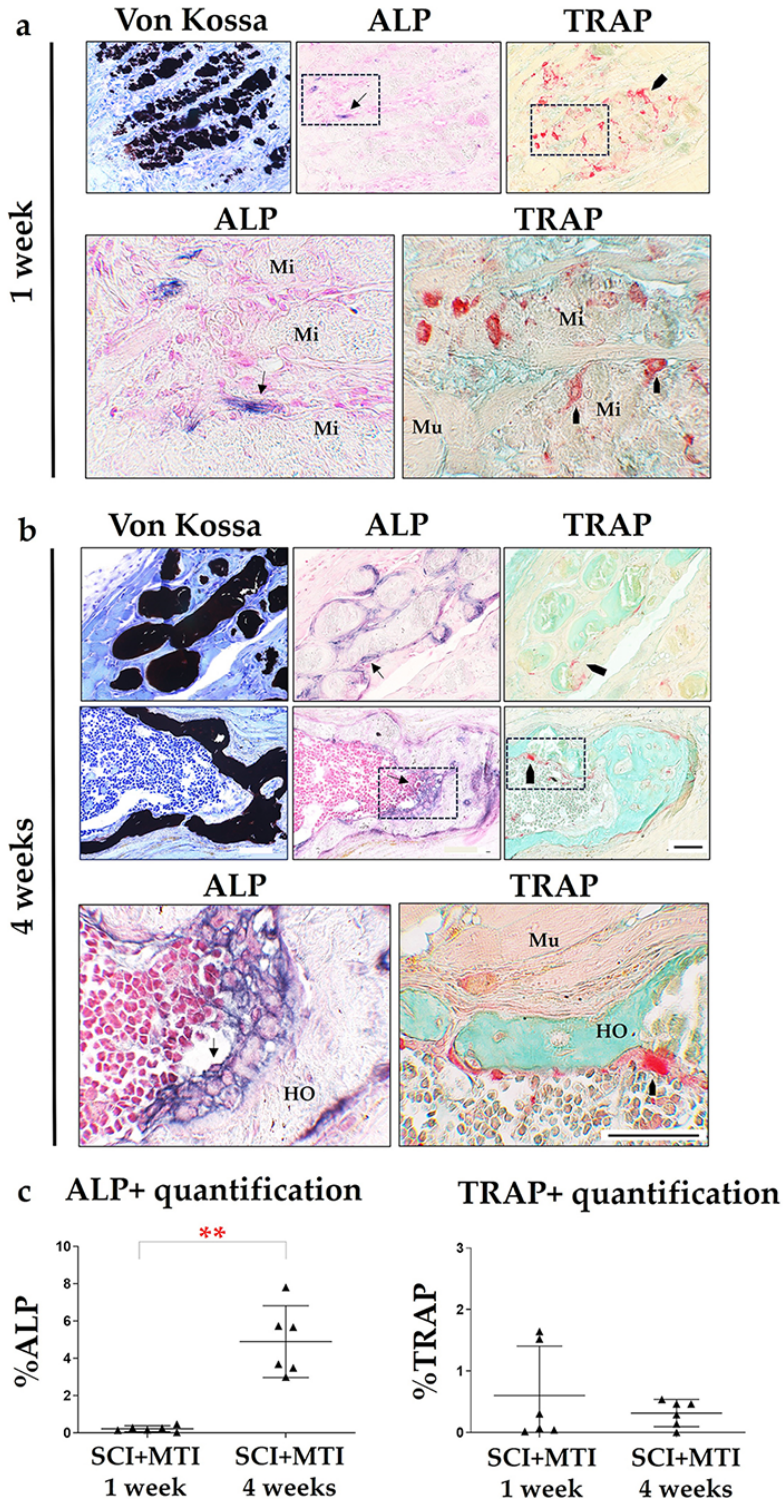

Fig. 4. Histochemical analysis of tissue and cellular activity in ectopic mineral deposition and bone formation in SCI+MTI mice. Consecutive 5-micron plastic embedded sections from 6 undecalcified SCI+MTI samples were used to correlate Von Kossa-stained mineral with alkaline phosphatase (ALP) activity and tartrate resistant acid phosphatase (TRAP) activity at 1 week and 4 weeks postoperative. At 1 week postoperative (**a**) von Kossa stained mineral deposits were associated with little ALP staining (arrow) and significant numbers of TRAP stained mononuclear cells (arrowhead). At 4 weeks postoperative (**b**) von Kossa stained mineral formed nodular structures embedded in muscle (upper panel) as well as trabeculae associated with marrow (lower panel). Both structures were lined with significant numbers of cuboidal ALP positive cells (arrows) and a few TRAP positive cells (arrowheads). Quantitative analyses (**c**) revealed a significant difference in ALP ($p < 0.01$) but not in TRAP activity. Mi, mineral; Mu, muscle. Scale bars in the lower magnification micrographs represent 1000 µm and 50 µm in the higher magnification micrographs. p **<0.01.

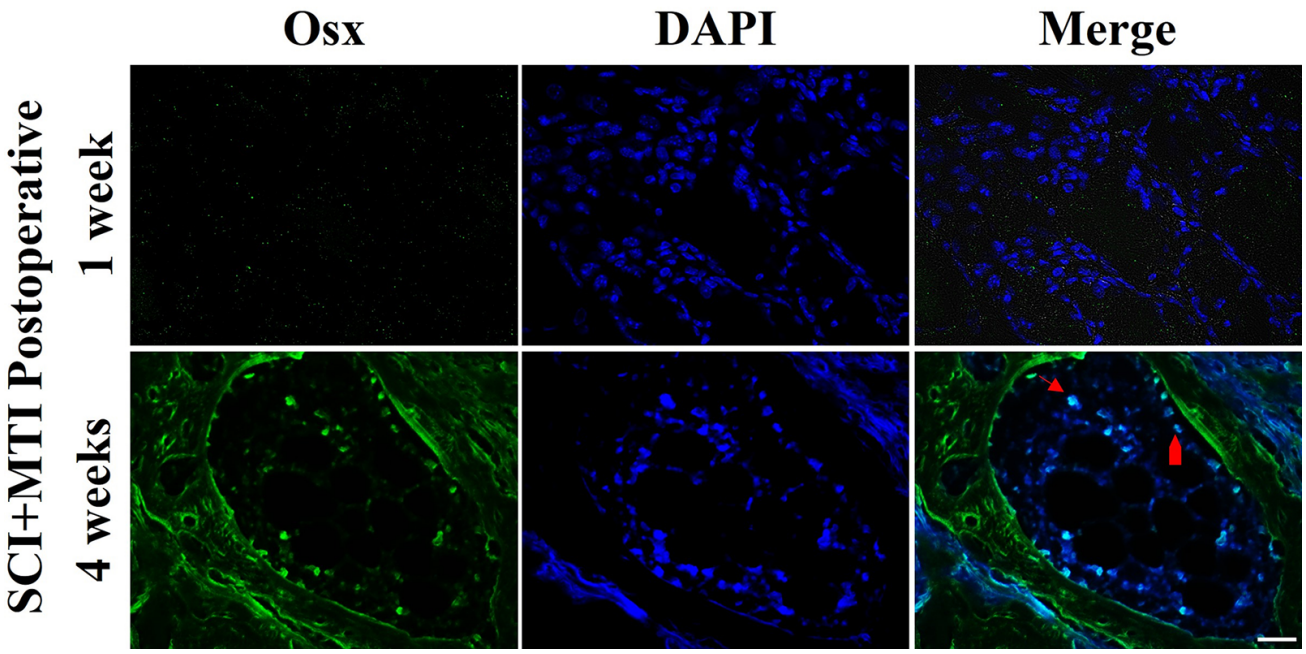

Fig. 5. Immunofluorescent staining of osteoblasts associated with ectopic mineral in SCI+MTI mice. Sections of decalcified hindlimbs were immunostained with antiserum that recognizes the transcription factor osterix (Osx) in osteoblast lineage cells and counterstained with DAPI nuclear stain. No Osx positive staining was seen around ectopic mineral deposits at 1 week postoperative. At 4 weeks postoperative osteoblasts were identified by co-localization of Osx positive staining with DAPI (turquoise). Scale bar represents 50 μm.

3**b**) and trabecular bone lined with cuboidal cells resembling osteoblasts at 4 weeks (Fig. 3**c**) postoperative.

As illustrated in Fig. 4, serial sections of undecalcified hindlimbs were used for histochemical analysis of SCI+MTI limbs stained with VK/TB, with alkaline phosphatase (ALP) or with tartrate-resistant acid phosphatase (TRAP). At 1 week postoperative (Fig. 4**a**) amorphous mineral was seen associated with low ALP activity (arrow) and higher TRAP activity (arrowhead). Higher magnification of the area within the squares indicated ALP and TRAP staining co-localised with mineral (Mi) deposits within muscle (Mu) and TRAP positive cells were mononuclear. At 4 weeks postoperative (Fig. 4**b**) VK/TB stained ectopic mineral assumed the form of nodules surrounded by mesenchyme and trabeculae enclosing marrow. Both structures were associated with increased ALP and consistent TRAP activity. Higher magnification of the area within the squares showed HO lined with numerous cuboidal ALP positive osteoblasts (arrow) and TRAP positive osteoclasts (arrowhead). Quantitative analyses confirmed the time-dependent increase in ALP staining while TRAP remained relatively stable from 1 to 4 weeks postoperative (Fig. 4**c**).

Fig. 5 presents immunofluorescent staining for the osteoblast transcription factor Osx with DAPI nuclear stain indicating no positive staining at 1 week postoperative in the injured left limb of SCI+MTI mice. By 4 weeks postoperative osteoblasts (turquoise) were identified along the surface of ectopic bone trabeculae (red arrowhead) and within the marrow cavity (red arrow).

As shown in Fig. 6, immunofluorescent staining for the macrophage marker F4/80 with DAPI nuclear stain indicated macrophage infiltration of mesenchyme was visible around ectopic mineral deposits in SCI+MTI limbs only at 1 week postoperative (Fig. 6**a**). Higher magnification of the areas within the red rectangles further confirmed the distribution of macrophages around the sites of mineral deposits (Fig. 6**b**).

In Fig. 7, the distal femur is shown with color-coded regions of interest (ROIs) used for quantitative micro-CT analysis (Fig. 7**a**) of orthotopic diaphyseal cortical bone (Fig. 7**b**) and metaphyseal trabecular bone (Fig. 7**c**). Representative 2D images of the left femora (Fig. 7**d**) reveal a reduction in metaphyseal trabecular bone (asterisk) and thinning of the proximal diaphyseal cortex (arrows) at 4 weeks postoperative in mice with SCI. Representative 3D reconstructions of distal femora of MTI (Fig. 7**e**) and SCI+MTI (Fig. 7**f**) mice indicate trabecular bone loss, attributable to a reduction in the number of trabeculae as well as trabecular thinning, and a reduction of the diaphyseal cortical thickness in SCI+MTI mice compared with MTI mice at 4 weeks postoperative.

As shown in Fig. 8**a**, quantitative micro-CT analyses of distal femora confirmed a significant loss of trabecular bone mass and BMD in both injured left and intact right metaphyses of mice with SCI+MTI compared to those with MTI at 4 weeks postoperative. Fig. 8**b** shows that cortical

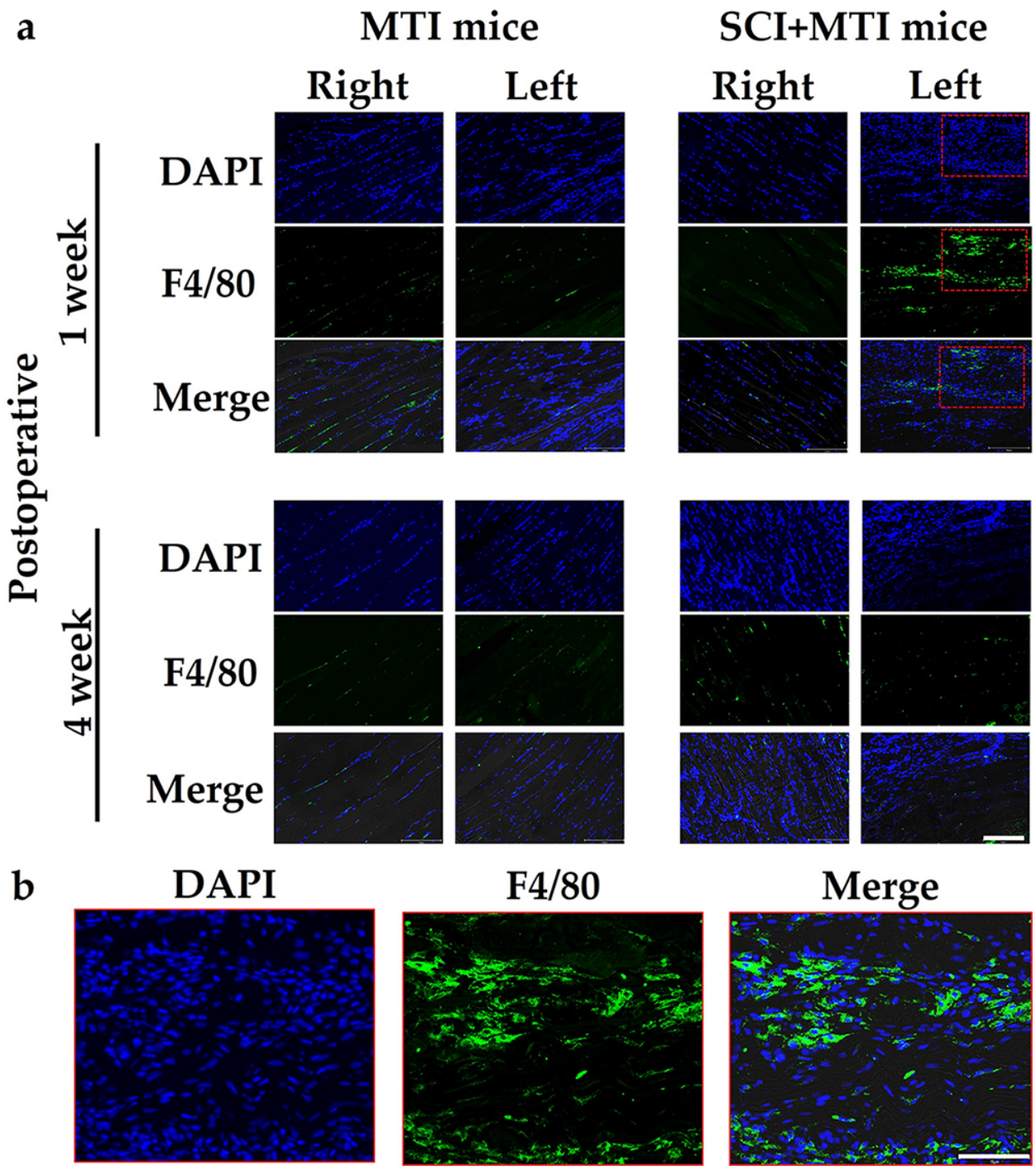

Fig. 6. Immunofluorescent staining of macrophages associated with ectopic mineral in MTI and SCI+MTI mice. Sections of decalcified limbs were immunostained with antiserum that recognizes F4/80 cell surface antigen on macrophage subtypes and counterstained with DAPI nuclear stain. Significant numbers of F4/80 positive cells (green) were seen infiltrating mesenchyme only at 1 week postoperative (**a**,**b**). Scale bar represents 150 μm in lower magnification images (**a**) and 75 μm in higher magnification images (**b**).

thinning and BMD reduction is also evident in the left and right femora of SCI+MTI mice at the same timepoint.

Discussion

Relevance of Previous Animal Models

A variety of animal models have been developed to study the pathogenesis of HO. One of the earliest models of trauma-induced HO involved injection of calcium chloride into the quadriceps muscle of rabbits (Heinen *et al.*, 1949). Subsequent research by orthopedic surgeon scientist Marshall R. Urist laid the groundwork for decades of research into the pathogenic mechanisms of HO. His contributions include experimental studies using rabbits which were used to provide radiologic and histologic evidence of

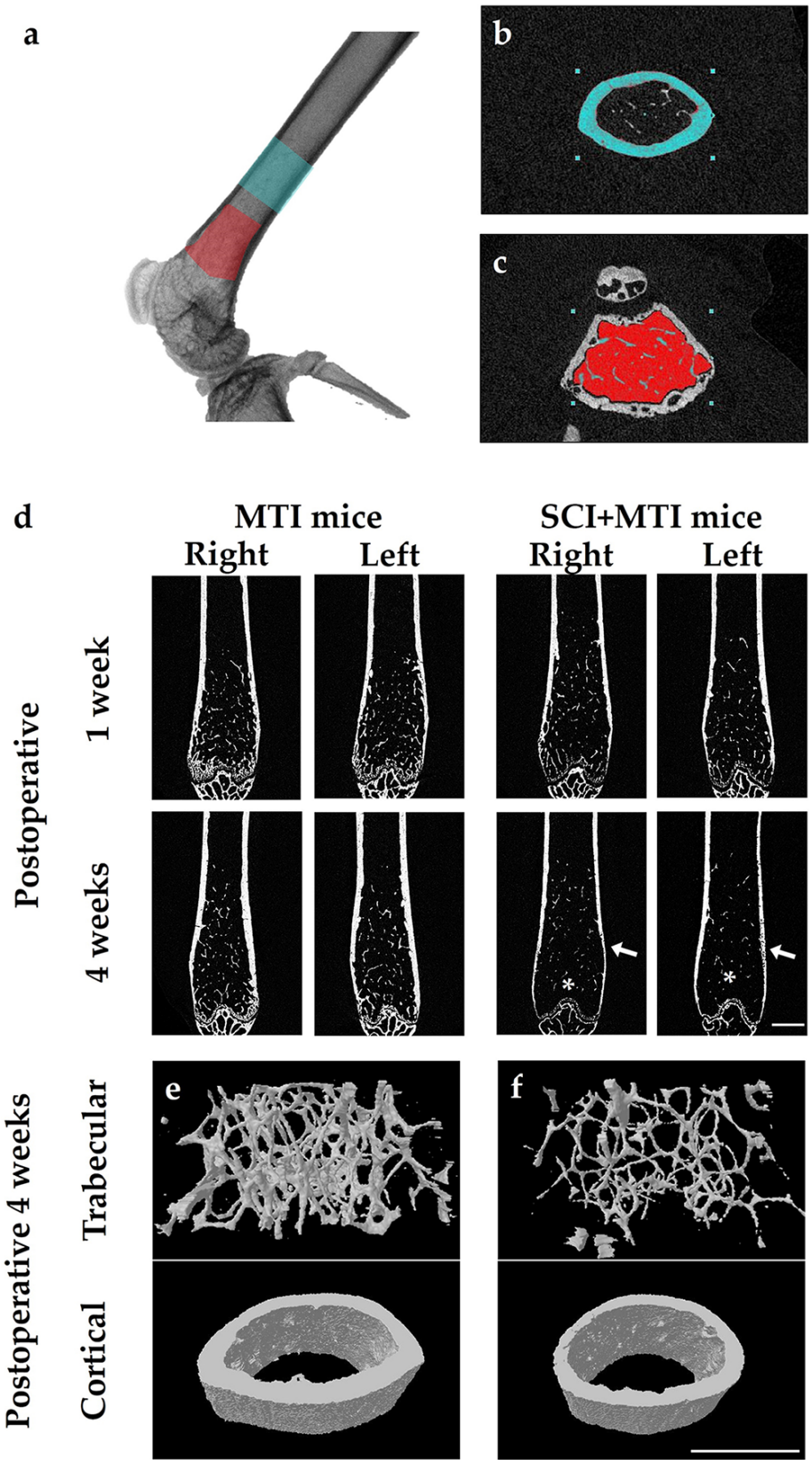

Fig. 7. Qualitative micro-CT analysis of distal femoral bone of MTI and SCI+MTI mice. The location of volumes of interest are shown in the context of the distal femur (**a**) and in transverse sections of cortical (**b**) and trabecular (**c**) bone. Representative 2D images of the distal femora (**d**) show reduced trabecular bone (asterisk) and cortical thinning (arrow) in both limbs of paralysed SCI+MTI mice, but not MTI mice at 4 weeks postoperative. 3D reconstruction of the 4 week specimens revealed thinning and loss of trabeculae and reduction of cortical thickness in SCI+MTI (**f**) compared with MTI mice (**e**). Scale bars represent 1 mm.

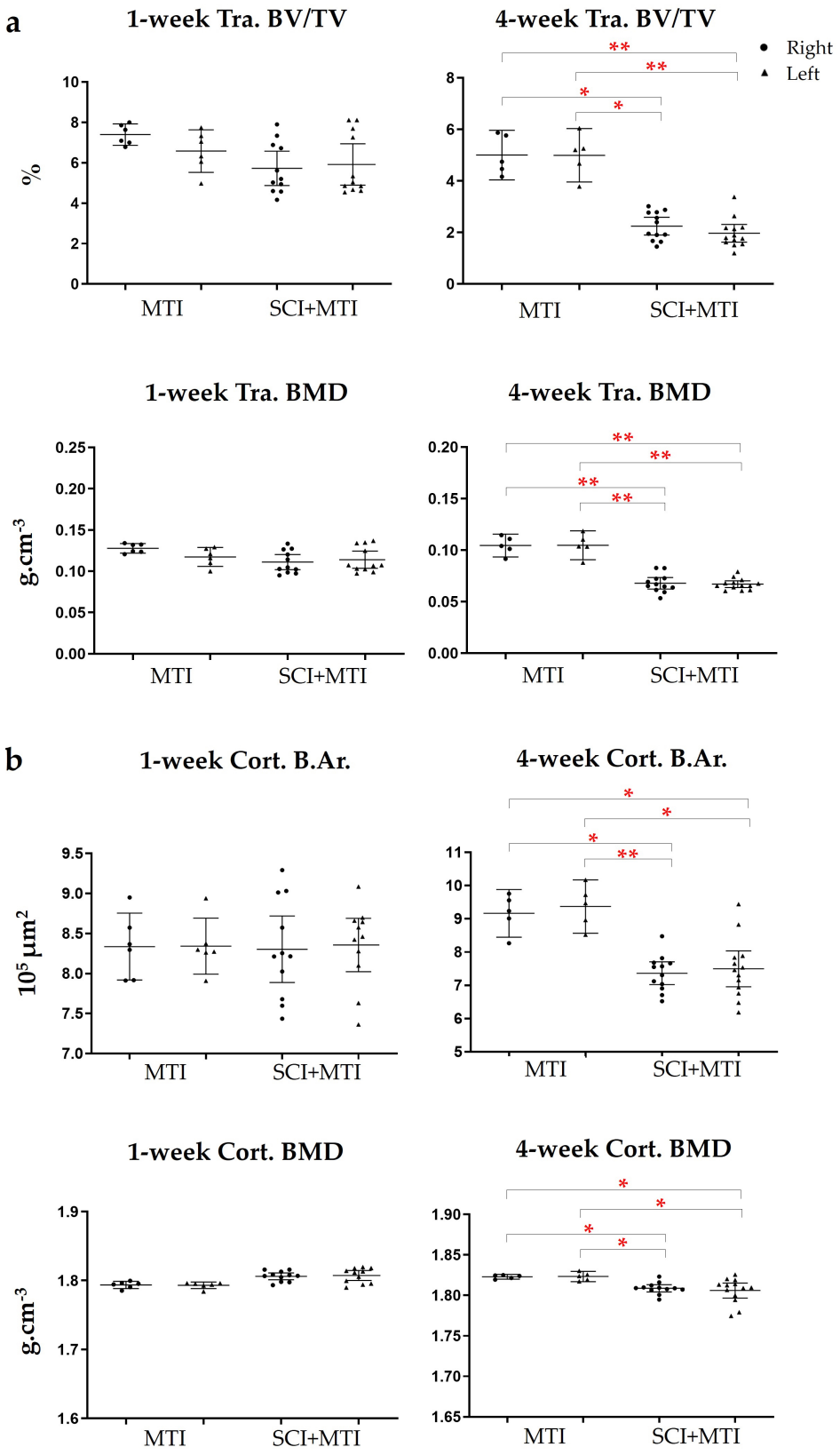

Fig. 8. Quantitative micro-CT analysis of distal femora of MTI and SCI+MTI mice. No significant differences in indices of trabecular (a: Tra BV/TV, Tra BMD) or cortical (b: Cort B.Ar, Cort BMD) bone quality were detected between the intact right and injured left femora of MTI or SCI+MTI mice at 1 week or 4 weeks postoperative. In contrast, significant reductions in both trabecular and cortical bone quality were noted between MTI and SCI+MTI at 4 weeks postoperative. p *<0.05, **<0.01.

HO in leg muscles after implantation of decalcified bone matrix (Urist, 1965). Additional studies identified host mesenchymal lineage cells and BMP sequestered in bone matrix as critical components for HO development (Urist *et al*., 1982). These foundational studies using rabbit models paved the way to the development and characterization by the military of a rat model of HO associated with blast injuries and amputations (Polfer *et al*., 2015; Qureshi *et al*., 2015). The limb injury involved a comminuted fracture of the femur with extensive muscle, vessel and nerve damage followed by amputation and quadriceps myoplasty. Micro-CT imaging, histologic analyses and gene profiling established a timeline for endochondral ossification and bone formation in the injured limb. The rat model was then used to attempt inhibition of ectopic bone by local intraoperative administration of vancomycin (Seavey *et al*., 2017).

Mouse models offer significant advantages in studying human diseases, primarily due to the ease with which their genetics can be modified. This facilitates a deeper understanding of the mechanisms underlying disease pathogenesis. Genetically modified mice were used with variable success to model heritable forms of HO (Chakkalakal *et al*., 2012; Hwang *et al*., 2022). Examples include the mouse models carrying receptor mutations found in human fibrodysplasia ossificans progressiva (FOP) (Lees-Shepard and Goldhamer, 2018; Yu *et al*., 2008) and those carrying inactivating mutations of Gnas, which encodes the α-subunit of the stimulatory G protein, observed in Albright's Hereditary Osteodystrophy (Castrop *et al*., 2007; Huso *et al*., 2011). Mice with targeted mutations in genes identified as key drivers of orthotopic bone formation have proven useful for identification of time dependent and tissue specific expression of regulators of HO (Hwang *et al*., 2022; Meyers *et al*., 2019). These genetic-based models of HO, whether utilized independently or in conjunction with traumatic injuries, highlight the complexity of the pathogenesis.

Mouse models of acquired HO secondary to muscle injury were induced by intramuscular injection of cardiotoxin, BMP2, or BMP9 (Leblanc *et al*., 2011; Lounev *et al*., 2009; Mignemi *et al*., 2017). Tendon injury in the form of repetitive crushing followed by tenotomy of Achilles tendon has also been used to study HO development in mice with conditional knockout of FGFR3 in chondrogenic cells (Zhang *et al*., 2021a). Combined injuries, consisting of burn and Achilles tenotomy were used to model burn-associated HO (Agarwal *et al*., 2017a). Targeted disruption of NGF/TrkA signaling was shown to reduce HO in these mice suggesting a neural component to its development (Lee *et al*., 2021). Injuries to central and peripheral nervous systems exaggerate the dystrophic calcification and HO formation resulting from intramuscular injection of cardiotoxin and BMP2 (Alexander *et al*., 2019; Debaud *et al*., 2017; Kang *et al*., 2014; Tőkési *et al*., 2020). These findings imply a significant neural element in the development of HO.

Less than 2 % of more than two thousand studies using animal models of SCI include musculoskeletal evaluation, and none recapitulate the musculotendinous injuries seen in individuals who sustain polytrauma with SCI (Sharif-Alhoseini *et al*., 2017). SCI-associated neurogenic HO has been modelled in mice by combining traumatic SCI with muscle injury induced by BMP2 loaded implants or cardiotoxin injection. These mouse models identified an essential role for simultaneous CNS and peripheral tissue injury in the induction of HO, albeit with muscle pathologies and healing mechanisms distinct from those arising from polytrauma. Therefore, this study presents a mouse model of polytrauma that was developed to accurately reflect the constellation of SCI associated injuries seen in clinical practice. In addition to HO, osteopenia was induced at 4 weeks postoperative in SCI+MTI mice. This was not unexpected as transection of the thoracic spinal cord resulted in long-term paraplegia and prolonged immobilization of the lower limbs leads to rapid breakdown of orthotopic bone (Koseki *et al*., 2022).

Regulation of Inflammation

Excessive and prolonged inflammation is proposed to play a central role in the development of traumatic HO. A review of the literature published over the past two decades revealed serum levels of astrocyte S100b and glial fibrillary acidic protein (GFAP) were transiently elevated while pro-inflammatory cytokines tumor necrosis factor (TNF)α and interleukin (IL)-6 remained elevated up to one year in patients with traumatic SCI (Leister *et al*., 2020). These clinical observations were supported by preclinical studies using rodent models in which expression of pro-inflammatory cytokines and infiltration of inflammatory cells remained elevated 14 days post-injury (Hellenbrand *et al*., 2021). In our model of SCI+MTI, F4/80 positive cells were recruited to the site of MTI at 1 week postoperative which aligns with the reported peak period of macrophage infiltration into damaged spinal cord. By 4 weeks postoperative there was little evidence of macrophage infiltration in the interstitial tissue surrounding HO lesions. Macrophages are instrumental in maintaining the balance between catabolic and anabolic activities during bone development by changing their phenotype in response to environmental cues (Horwood, 2016). Different subsets of macrophages promote HO formation via distinct molecular mechanisms that involve regulation of tissue inflammation, hypoxia and angiogenesis, as well as osteogenic differentiation of precursor cells (Huang *et al*., 2021). In mouse models of Achilles tenotomy, macrophages were shown to drive HO by activating the TNFα-mTOR signalling pathway (Kushima *et al*., 2023). Others used a mouse model of extensive burn injury to demonstrate a role for macrophage derived TGFβ1 in HO development (Sorkin *et al*., 2020). M1 macrophages were identified as a source of BMP-2 that contributes to vascular smooth muscle mineralization (Dube *et al*., 2017) and an

M2 subset identified by molecular profiling to contribute to orthotopic and heterotopic bone formation (Olmsted-Davis *et al*., 2021). Macrophage derived Oncostatin-M (Torossian *et al*., 2017) and IL-1 isoforms (Tseng *et al*., 2022) have both been implicated in neurogenic HO associated with traumatic SCI in humans and mice. Taken together these studies provide some insight into the complexity of growth factor and cytokine signalling pathways that contribute to HO.

In our SCI+MTI model, TRAP activity was present in mononuclear cells adjacent to mineral deposits at 1 week postoperative in the absence of significant ALP staining. TRAP is expressed by macrophages as well as dendritic cells and osteoclasts, and capable of hydrolysing substrates to generate reactive oxygen species (Hayman, 2008). Given the absence of significant ALP activity in damaged muscle at postoperative 1 week in our model of SCI+MTI, the TRAP-positive mononuclear cells seen were most likely macrophages rather than osteoclasts. Inflammatory M1 macrophages release the TRAP5a isoform whereas osteoclasts release TRAP5b (Janckila *et al*., 2007). Lineage tracing studies identified yolk-sac-derived TRAP-positive macrophages that are stored in the spleen and released into the circulation and migrate to the site of a femoral drill hole defect in young adult mice (Yahara *et al*., 2020). Their relationship to the multinucleate TRAP-positive cells, which colocalize with ALP-positive cells involved in bone turnover in marrow cavities at 4 weeks postoperative remains to be defined.

Ectopic Mineralization

Biomineralization is a process involving the interaction between matrix proteins and minerals. Orthotopic ossification is the physiologic process of calcium phosphate (hydroxyapatite) mineral deposition during the development of bones and teeth, and during post-natal repair of stabilized fractures (Murshed, 2018). Heterotopic or ectopic mineralization, also known as dystrophic calcification (DC), describes the pathophysiologic process of calcium mineral deposition in soft tissues, including heart muscle (Alyesh *et al*., 2019), vascular smooth muscle (Proudfoot, 2019), skeletal muscle (Moore-Lotridge *et al*., 2019), tendons (O'Brien *et al*., 2012) and ligaments (Fournier *et al*., 2020). It has been proposed that HO initiates as DC in these tissues following injury when normal inhibitory mechanisms are disrupted.

It is possible the fibrin deposited at the MTI site in the paralytic hindlimb of our model acts as a matrix platform for hydroxyapatite deposition. SCI is commonly complicated by dysregulation of hemostasis and thrombosis (Moore *et al*., 2021). While the molecular mechanisms underlying trauma-induced coagulopathy remain largely undefined, reduced fibrinolysis has been proposed as a unifying factor driving trauma-related HO (Li and Tuan, 2020). This hypothesis was tested using long bone fractures in *Plg-/-* mice with excess circulating fibrin arising from targeted disruption of the plasminogen gene (Yuasa *et al*., 2015) and in wild-type mice with muscle injury and pharmacologic plasmin inhibition (Mignemi *et al*., 2017).

Pyrophosphoric acid (PPi) is also recognized as a potent anti-mineralization agent, so the balance between PPi and inorganic phosphate (Pi) can influence tissue mineralization. Proinflammatory M1 macrophages have low expression levels of the enzyme ENPP1 involved in the synthesis of PPi (Villa-Bellosta *et al*., 2016). In contrast, expression of the enzyme ENTPD1 involved in release of Pi from ATP and ADP hydrolysis is high. The resultant decrease in the PPi/Pi ratio could be another mechanism driving mineral deposition in our model in the first week postoperative.

Potential Sources of Osteogenic and Osteolytic Cells in Traumatic HO

Mineral deposition in connective tissue requires the soluble factors, discussed above, to provide an osteoinductive microenvironment and a source of osteogenic cells. The MTI in our model involved muscle, nerve, blood vessel, and tendon injury, all of which have been identified as potential sources of osteogenic progenitor cells in humans and mice (Meyers *et al*., 2019). Although mice with SCI+MTI showed a tendency toward increased ectopic mineral volume compared to SCI+MI mice, the difference did not reach significance, most likely due to the large intra-group variability. This implies that stem cells from both muscle and tendon played a role in HO formation in our model. Skeletal muscle progenitor cells were recently shown to express intracellular tissue non-specific ALP rather than at the cell surface, where it performs its prototypical role in skeletal mineralization (Zhang *et al*., 2021b). Alternatively, it is possible that the ALP-positive cells were bone marrow-derived circulating osteoprogenitors (Feehan *et al*., 2021), as demonstrated in a mouse model of BMP-induced HO (Otsuru *et al*., 2007). In human samples of early-stage SCI-associated HO, circulating osteoprogenitors were identified in the fibroproliferative and neovascular regions (Egan *et al*., 2018). Our histologic analysis of damaged muscle at 4 weeks postoperative indicated nodular mineral deposits accompanied by scattered ALP and TRAP-positive cells. The ALP-positive cells seen at four weeks lining bone adjacent to bone marrow were no doubt osteogenic.

Limitations

Although males account for 83.2 % of patients with traumatic SCI (Kim *et al*., 2021), only female mice were used for our experiments to avoid blockage of the urinary tract in male mice, as seen in our pilot study. Urinary retention in SCI+MTI mice throughout the postoperative course required manual bladder compression to achieve bladder emptying. The longer urethra and associated higher re-

sistance predisposed male mice to develop urinary blockage that led to a high rate of euthanasia for humane endpoints in our pilot study. An alternative approach to model SCI+MTI in male mice would be to induce incomplete SCI by spinal cord contusion (Graham *et al*., 2021) or hemisection (Battistuzzo *et al*., 2016). As described mice with incomplete SCI were reported to regain voiding function within 2 weeks (Mure *et al*., 2004). Another limitation of this study is the lack of objective measurement of the crush force applied to the quadriceps muscle. Future studies could include adult male mice, in keeping with the clinical prevalence of the disorder, to elucidate the impact of sex hormones on HO development in SCI+MTI mice.

Conclusion

Shortcomings in existing models led us to develop a new, clinically relevant mouse model of polytrauma with SCI+MTI co-morbidities. Ectopic mineralization was restricted to the MTI site and associated with macrophage infiltration in the surrounding area at 1 week postoperative. Heterotopic bone accompanied by ALP and TRAP-positive cells lining marrow cavities formed in the presence of long-term SCI-induced paralysis and disuse osteopenia at 4 weeks postoperative. Taken together, the results resemble those documented in humans with SCI-associated HO and disuse osteopenia. Heterotopic bone and loss of orthotopic bone occurred in 100 % of surgically modified mice. The model and the analytic tools can thus serve as a preclinical platform to test novel therapeutic approaches to inhibit HO associated with traumatic injuries.

List of Abbreviations

ALP, alkaline phosphatase; AUP, animal use protocol; BMP, bone morphogenetic protein; CCAC, Canadian Council on Animal Care; CNS, central nervous system; CO_2, carbon dioxide; DC, dystrophic calcification; ENPP, ecto-nucleotide pyrophosphatase/phosphodiesterase; GFAP, glial fibrillary acidic protein; HO, heterotopic ossification; IL-6, interleukin-6; IQR, interquartile range; MMA, methyl methacrylate; Micro-CT, micro-computed tomography; MTI, myotendinous injury; NGF, nerve growth factor; PBS, phosphate-buffered saline; PPi, pyrophosphate; RI-MUHC, Research Institute of McGill University Health Centre; ROI, region of interest; SCI, spinal cord injury; T9-T10, thoracic vertebrae 9-10; TBI, traumatic brain injury; TNFα, tumor necrosis factor α and interleukin; TRAP, tartrate-resistant acid phosphatase; TrkA, tropomyosin receptor kinase A; VK/TB, Von Kossa/Toluidine Blue.

Availability of Data and Materials

The data that substantiate the conclusions of this study can be obtained from the corresponding author CG.

Author Contributions

Planning of the study was performed by GSJ, MR, RG and CG. Data collection was performed by RA, GU, TK, JAP, and CG. Data analysis was performed by RA, GU, TK, JAP, RG and CG. Manuscript was prepared and edited by RA, TK, GSJ, MR, RG and CG. Manuscript was finalized and resubmitted after revision by RA and CG. All authors contributed to editorial changes in the manuscript, All authors read and approved the final manuscript. All authors have participated sufficiently in the work and agreed to be accountable for all aspects of the work.

Ethics Approval and Consent to Participate

All mouse procedures were approved for use by the Facility Animal Care Committee of McGill University (AUP 2021-8214) in accordance with the policies and guidelines of the Canadian Council on Animal Care (CCAC).

Acknowledgments

The authors gratefully acknowledge the assistance of Ailian Li for the histological study, Laura Curran from Dr. Sam David's lab for SCI mouse model development, and Dr. Monzur Murshed for model characterization.

Funding

Fonds de Recherche du Québec - Santé (FRQS)-sponsored Le Réseau de recherche en santé buccodentaire et osseuse (RSBO), AO Spine North America (YIRGA2022), AO Spine (22-050), North American Spine Society (NASS), Montreal General Hospital (MGH) Foundation, McGill University Department of Medicine, and Research Institute of the McGill University Health Centre (RI-MUHC).

Conflict of Interest

The authors declare no conflict of interest.

References

Agarwal S, Loder SJ, Cholok D, Peterson J, Li J, Breuler C, Cameron Brownley R, Hsin Sung H, Chung MT, Kamiya N, Li S, Zhao B, Kaartinen V, Davis TA, Qureshi AT, Schipani E, Mishina Y, Levi B (2017a) Scleraxis-Lineage Cells Contribute to Ectopic Bone Formation in Muscle and Tendon. Stem Cells (Dayton, Ohio) 35: 705-710. DOI: 10.1002/stem.2515.

Agarwal S, Sorkin M, Levi B (2017b) Heterotopic Ossification and Hypertrophic Scars. Clinics in Plastic Surgery 44: 749-755. DOI: 10.1016/j.cps.2017.05.006.

Alexander KA, Tseng HW, Fleming W, Jose B, Salga M, Kulina I, Millard SM, Pettit AR, Genêt F, Levesque JP (2019) Inhibition of JAK1/2 Tyrosine Kinases Reduces Neurogenic Heterotopic Ossification After Spinal Cord Injury. Frontiers in Immunology 10: 377. DOI:

10.3389/fimmu.2019.00377.

Alyesh DM, Siontis KC, Sharaf Dabbagh G, Yokokawa M, Njeim M, Patel S, Morady F, Bogun F (2019) Postinfarction Myocardial Calcifications on Cardiac Computed Tomography: Implications for Mapping and Ablation in Patients With Nontolerated Ventricular Tachycardias. Circulation. Arrhythmia and Electrophysiology 12: e007023. DOI: 10.1161/CIRCEP.118.007023.

Ampadiotaki MM, Evangelopoulos DS, Pallis D, Vlachos C, Vlamis J, Evangelopoulos ME (2021) New Strategies in Neurogenic Heterotopic Ossification. Cureus 13: e14709. DOI: 10.7759/cureus.14709.

Arduini M, Mancini F, Farsetti P, Piperno A, Ippolito E (2015) A new classification of peri-articular heterotopic ossification of the hip associated with neurological injury: 3D CT scan assessment and intra-operative findings. The Bone & Joint Journal 97-B: 899-904. DOI: 10.1302/0301-620X.97B7.35031.

Banovac K, Sherman AL, Estores IM, Banovac F (2004) Prevention and treatment of heterotopic ossification after spinal cord injury. The Journal of Spinal Cord Medicine 27: 376-382. DOI: 10.1080/10790268.2004.11753775.

Battistuzzo CR, Rank MM, Flynn JR, Morgan DL, Callister R, Callister RJ, Galea MP (2016) Gait recovery following spinal cord injury in mice: Limited effect of treadmill training. The Journal of Spinal Cord Medicine 39: 335-343. DOI: 10.1080/10790268.2015.1133017.

Behrends DA, Cheng L, Sullivan MB, Wang MH, Roby GB, Zayed N, Gao C, Henderson JE, Martineau PA (2014) Defective bone repair in mast cell deficient mice with c-Kit loss of function. European Cells & Materials 28: 209-209–21; discussion 221–2. DOI: 10.22203/ecm.v028a14.

Castrop H, Oppermann M, Mizel D, Huang Y, Faulhaber-Walter R, Weiss Y, Weinstein LS, Chen M, Germain S, Lu H, Ragland D, Schimel DM, Schnermann J (2007) Skeletal abnormalities and extra-skeletal ossification in mice with restricted Gsalpha deletion caused by a renin promoter-Cre transgene. Cell and Tissue Research 330: 487-501. DOI: 10.1007/s00441-007-0491-6.

Chakkalakal SA, Zhang D, Culbert AL, Convente MR, Caron RJ, Wright AC, Maidment ADA, Kaplan FS, Shore EM (2012) An Acvr1 R206H knock-in mouse has fibrodysplasia ossificans progressiva. Journal of Bone and Mineral Research: the Official Journal of the American Society for Bone and Mineral Research 27: 1746-1756. DOI: 10.1002/jbmr.1637.

Debaud C, Salga M, Begot L, Holy X, Chedik M, de l'Escalopier N, Torossian F, Levesque JP, Lataillade JJ, Le Bousse-Kerdilès MC, Genêt F (2017) Peripheral denervation participates in heterotopic ossification in a spinal cord injury model. PloS One 12: e0182454. DOI: 10.1371/journal.pone.0182454.

Denormandie P, de l'Escalopier N, Gatin L, Grelier A, Genêt F (2018) Resection of neurogenic heterotopic ossification (NHO) of the hip. Orthopaedics & Traumatology, Surgery & Research: OTSR 104: S121-S127. DOI: 10.1016/j.otsr.2017.04.015.

Dube PR, Birnbaumer L, Vazquez G (2017) Evidence for constitutive bone morphogenetic protein-2 secretion by M1 macrophages: Constitutive auto/paracrine osteogenic signaling by BMP-2 in M1 macrophages. Biochemical and Biophysical Research Communications 491: 154-158. DOI: 10.1016/j.bbrc.2017.07.065.

Egan KP, Duque G, Keenan MA, Pignolo RJ (2018) Circulating osteogentic precursor cells in non-hereditary heterotopic ossification. Bone 109: 61-64. DOI: 10.1016/j.bone.2017.12.028.

Feehan J, Nurgali K, Apostolopoulos V, Duque G (2021) Development and validation of a new method to isolate, expand, and differentiate circulating osteogenic precursor (COP) cells. Bone Reports 15: 101109. DOI: 10.1016/j.bonr.2021.101109.

Fournier DE, Kiser PK, Beach RJ, Dixon SJ, Séguin CA (2020) Dystrophic calcification and heterotopic ossification in fibrocartilaginous tissues of the spine in diffuse idiopathic skeletal hyperostosis (DISH). Bone Research 8: 16. DOI: 10.1038/s41413-020-0091-6.

Gao C, Harvey EJ, Chua M, Chen BP, Jiang F, Liu Y, Li A, Wang H, Henderson JE (2013) MSC-seeded dense collagen scaffolds with a bolus dose of VEGF promote healing of large bone defects. European Cells & Materials 26: 195-207; discussion 207. DOI: 10.22203/ecm.v026a14.

Gao C, Seuntjens J, Kaufman GN, Tran-Khanh N, Butler A, Li A, Wang H, Buschmann MD, Harvey EJ, Henderson JE (2012) Mesenchymal stem cell transplantation to promote bone healing. Journal of Orthopaedic Research: Official Publication of the Orthopaedic Research Society 30: 1183-1189. DOI: 10.1002/jor.22028.

Genêt F, Denormandie P, Keenan MA (2019) Orthopaedic surgery for patients with central nervous system lesions: Concepts and techniques. Annals of Physical and Rehabilitation Medicine 62: 225-233. DOI: 10.1016/j.rehab.2018.09.004.

Genêt F, Kulina I, Vaquette C, Torossian F, Millard S, Pettit AR, Sims NA, Anginot A, Guerton B, Winkler IG, Barbier V, Lataillade JJ, Le Bousse-Kerdilès MC, Hutmacher DW, Levesque JP (2015) Neurological heterotopic ossification following spinal cord injury is triggered by macrophage-mediated inflammation in muscle. The Journal of Pathology 236: 229-240. DOI: 10.1002/path.4519.

Graham ZA, DeBerry JJ, Cardozo CP, Bamman MM (2021) A 50 kdyne contusion spinal cord injury with or without the drug SS-31 was not associated with major changes in muscle mass or gene expression 14 d after injury in young male mice. Physiological Reports 9: e14751. DOI: 10.14814/phy2.14751.

Hardy D, Besnard A, Latil M, Jouvion G, Briand D, Thépenier C, Pascal Q, Guguin A, Gayraud-Morel B,

Cavaillon JM, Tajbakhsh S, Rocheteau P, Chrétien F (2016) Comparative Study of Injury Models for Studying Muscle Regeneration in Mice. PloS One 11: e0147198. DOI: 10.1371/journal.pone.0147198.

Hayman AR (2008) Tartrate-resistant acid phosphatase (TRAP) and the osteoclast/immune cell dichotomy. Autoimmunity 41: 218-223. DOI: 10.1080/08916930701694667.

Heinen JH, Jr, DABBS GH, MASON HA (1949) The experimental production of ectopic cartilage and bone in the muscles of rabbits. The Journal of Bone and Joint Surgery. American Volume 31A: 765-775.

Hellenbrand DJ, Quinn CM, Piper ZJ, Morehouse CN, Fixel JA, Hanna AS (2021) Inflammation after spinal cord injury: a review of the critical timeline of signaling cues and cellular infiltration. Journal of Neuroinflammation 18: 284. DOI: 10.1186/s12974-021-02337-2.

Horwood NJ (2016) Macrophage Polarization and Bone Formation: A review. Clinical Reviews in Allergy & Immunology 51: 79-86. DOI: 10.1007/s12016-015-8519-2.

Huang Y, Wang X, Zhou D, Zhou W, Dai F, Lin H (2021) Macrophages in heterotopic ossification: from mechanisms to therapy. NPJ Regenerative Medicine 6: 70. DOI: 10.1038/s41536-021-00178-4.

Huso DL, Edie S, Levine MA, Schwindinger W, Wang Y, Jüppner H, Germain-Lee EL (2011) Heterotopic ossifications in a mouse model of albright hereditary osteodystrophy. PloS One 6: e21755. DOI: 10.1371/journal.pone.0021755.

Hwang CD, Pagani CA, Nunez JH, Cherief M, Qin Q, Gomez-Salazar M, Kadaikal B, Kang H, Chowdary AR, Patel N, James AW, Levi B (2022) Contemporary perspectives on heterotopic ossification. JCI Insight 7: e158996. DOI: 10.1172/jci.insight.158996.

Janckila AJ, Slone SP, Lear SC, Martin A, Yam LT (2007) Tartrate-resistant acid phosphatase as an immunohistochemical marker for inflammatory macrophages. American Journal of Clinical Pathology 127: 556-566. DOI: 10.1309/DGEA9BE2VE5VCFYH.

Kang H, Dang ABC, Joshi SK, Halloran B, Nissenson R, Zhang X, Li J, Kim HT, Liu X (2014) Novel mouse model of spinal cord injury-induced heterotopic ossification. Journal of Rehabilitation Research and Development 51: 1109-1118. DOI: 10.1682/JRRD.2014.01.0019.

Kim HS, Lim KB, Kim J, Kang J, Lee H, Lee SW, Yoo J (2021) Epidemiology of Spinal Cord Injury: Changes to Its Cause Amid Aging Population, a Single Center Study. Annals of Rehabilitation Medicine 45: 7-15. DOI: 10.5535/arm.20148.

Körmendi S, Vecsei B, Ambrus S, Orhan K, Dobó-Nagy C (2021) Evaluation of the effect of vitamin D3 on mandibular condyles in an ovariectomized mouse model: a micro-CT study. BMC Oral Health 21: 627. DOI: 10.1186/s12903-021-01980-8.

Koseki H, Osaki M, Honda Y, Sunagawa S, Imai C, Shida T, Matsumura U, Sakamoto J, Tomonaga I, Yokoo S, Mizukami S, Okita M (2022) Progression of microstructural deterioration in load-bearing immobilization osteopenia. PloS One 17: e0275439. DOI: 10.1371/journal.pone.0275439.

Kushima Y, Sato Y, Kobayashi T, Fukuma Y, Matsumoto M, Nakamura M, Iwamoto T, Miyamoto T (2023) TNFα-dependent mTOR activity is required for tenotomy-induced ectopic ossification in mice. Journal of Bone and Mineral Metabolism 41: 583-591. DOI: 10.1007/s00774-023-01437-8.

Lacourt M, Gao C, Li A, Girard C, Beauchamp G, Henderson JE, Laverty S (2012) Relationship between cartilage and subchondral bone lesions in repetitive impact trauma-induced equine osteoarthritis. Osteoarthritis and Cartilage 20: 572-583. DOI: 10.1016/j.joca.2012.02.004.

Leblanc E, Trensz F, Haroun S, Drouin G, Bergeron E, Penton CM, Montanaro F, Roux S, Faucheux N, Grenier G (2011) BMP-9-induced muscle heterotopic ossification requires changes to the skeletal muscle microenvironment. Journal of Bone and Mineral Research: the Official Journal of the American Society for Bone and Mineral Research 26: 1166-1177. DOI: 10.1002/jbmr.311.

Lee S, Hwang C, Marini S, Tower RJ, Qin Q, Negri S, Pagani CA, Sun Y, Stepien DM, Sorkin M, Kubiak CA, Visser ND, Meyers CA, Wang Y, Rasheed HA, Xu J, Miller S, Huber AK, Minichiello L, Cederna PS, Kemp SWP, Clemens TL, James AW, Levi B (2021) NGF-TrkA signaling dictates neural ingrowth and aberrant osteochondral differentiation after soft tissue trauma. Nature Communications 12: 4939. DOI: 10.1038/s41467-021-25143-z.

Lees-Shepard JB, Goldhamer DJ (2018) Stem cells and heterotopic ossification: Lessons from animal models. Bone 109: 178-186. DOI: 10.1016/j.bone.2018.01.029.

Łęgosz P, Otworowski M, Sibilska A, Starszak K, Kotrych D, Kwapisz A, Synder M (2019) Heterotopic Ossification: A Challenging Complication of Total Hip Arthroplasty: Risk Factors, Diagnosis, Prophylaxis, and Treatment. BioMed Research International 2019: 3860142. DOI: 10.1155/2019/3860142.

Leister I, Haider T, Mattiassich G, Kramer JLK, Linde LD, Pajalic A, Grassner L, Altendorfer B, Resch H, Aschauer-Wallner S, Aigner L (2020) Biomarkers in Traumatic Spinal Cord Injury-Technical and Clinical Considerations: A Systematic Review. Neurorehabilitation and Neural Repair 34: 95-110. DOI: 10.1177/1545968319899920.

Li L, Tuan RS (2020) Mechanism of traumatic heterotopic ossification: In search of injury-induced osteogenic factors. Journal of Cellular and Molecular Medicine 24: 11046-11055. DOI: 10.1111/jcmm.15735.

Lounev VY, Ramachandran R, Wosczyna MN, Yamamoto M, Maidment ADA, Shore EM, Glaser DL, Goldhamer DJ, Kaplan FS (2009) Identification of progenitor cells that contribute to heterotopic skeletogenesis. The

Journal of Bone and Joint Surgery. American Volume 91: 652-663. DOI: 10.2106/JBJS.H.01177.

Meyers C, Lisiecki J, Miller S, Levin A, Fayad L, Ding C, Sono T, McCarthy E, Levi B, James AW (2019) Heterotopic Ossification: A Comprehensive Review. JBMR Plus 3: e10172 DOI: 10.1002/jbm4.10172.

Mignemi NA, Yuasa M, Baker CE, Moore SN, Ihejirika RC, Oelsner WK, Wallace CS, Yoshii T, Okawa A, Revenko AS, MacLeod AR, Bhattacharjee G, Barnett JV, Schwartz HS, Degen JL, Flick MJ, Cates JM, Schoenecker JG (2017) Plasmin Prevents Dystrophic Calcification After Muscle Injury. Journal of Bone and Mineral Research: the Official Journal of the American Society for Bone and Mineral Research 32: 294-308. DOI: 10.1002/jbmr.2973.

Moore-Lotridge SN, Li Q, Gibson BHY, Martin JT, Hawley GD, Arnold TH, Saito M, Tannouri S, Schwartz HS, Gumina RJ, Cates JMM, Uitto J, Schoenecker JG (2019) Trauma-Induced Nanohydroxyapatite Deposition in Skeletal Muscle is Sufficient to Drive Heterotopic Ossification. Calcified Tissue International 104: 411-425. DOI: 10.1007/s00223-018-0502-5.

Moore EE, Moore HB, Kornblith LZ, Neal MD, Hoffman M, Mutch NJ, Schöchl H, Hunt BJ, Sauaia A (2021) Trauma-induced coagulopathy. Nature Reviews. Disease Primers 7: 30. DOI: 10.1038/s41572-021-00264-3.

Mure PY, Galdo M, Compagnone N (2004) Bladder function after incomplete spinal cord injury in mice: quantifiable outcomes associated with bladder function and efficiency of dehydroepiandrosterone as a therapeutic adjunct. Journal of Neurosurgery 100: 56-61. DOI: 10.3171/spi.2004.100.1.0056.

Murshed M (2018) Mechanism of Bone Mineralization. Cold Spring Harbor Perspectives in Medicine 8: a031229. DOI: 10.1101/cshperspect.a031229.

O'Brien EJO, Frank CB, Shrive NG, Hallgrímsson B, Hart DA (2012) Heterotopic mineralization (ossification or calcification) in tendinopathy or following surgical tendon trauma. International Journal of Experimental Pathology 93: 319-331. DOI: 10.1111/j.1365-2613.2012.00829.x.

Olmsted-Davis E, Mejia J, Salisbury E, Gugala Z, Davis AR (2021) A Population of M2 Macrophages Associated With Bone Formation. Frontiers in Immunology 12: 686769. DOI: 10.3389/fimmu.2021.686769.

Otsuru S, Tamai K, Yamazaki T, Yoshikawa H, Kaneda Y (2007) Bone marrow-derived osteoblast progenitor cells in circulating blood contribute to ectopic bone formation in mice. Biochemical and Biophysical Research Communications 354: 453-458. DOI: 10.1016/j.bbrc.2006.12.226.

Polfer EM, Hope DN, Elster EA, Qureshi AT, Davis TA, Golden D, Potter BK, Forsberg JA (2015) The development of a rat model to investigate the formation of blast-related post-traumatic heterotopic ossification. The Bone & Joint Journal 97-B: 572-576. DOI: 10.1302/0301-620X.97B4.34866.

Proudfoot D (2019) Calcium Signaling and Tissue Calcification. Cold Spring Harbor Perspectives in Biology 11: a035303. DOI: 10.1101/cshperspect.a035303.

Qureshi AT, Crump EK, Pavey GJ, Hope DN, Forsberg JA, Davis TA (2015) Early Characterization of Blast-related Heterotopic Ossification in a Rat Model. Clinical Orthopaedics and Related Research 473: 2831-2839. DOI: 10.1007/s11999-015-4240-y.

Seavey JG, Wheatley BM, Pavey GJ, Tomasino AM, Hanson MA, Sanders EM, Dey D, Moss KL, Potter BK, Forsberg JA, Qureshi AT, Davis TA (2017) Early local delivery of vancomycin suppresses ectopic bone formation in a rat model of trauma-induced heterotopic ossification. Journal of Orthopaedic Research: Official Publication of the Orthopaedic Research Society 35: 2397-2406. DOI: 10.1002/jor.23544.

Sharif-Alhoseini M, Khormali M, Rezaei M, Safdarian M, Hajighadery A, Khalatbari MM, Safdarian M, Meknatkhah S, Rezvan M, Chalangari M, Derakhshan P, Rahimi-Movaghar V (2017) Animal models of spinal cord injury: a systematic review. Spinal Cord 55: 714-721. DOI: 10.1038/sc.2016.187.

Sorkin M, Huber AK, Hwang C, Carson WF, 4th, Menon R, Li J, Vasquez K, Pagani C, Patel N, Li S, Visser ND, Niknafs Y, Loder S, Scola M, Nycz D, Gallagher K, McCauley LK, Xu J, James AW, Agarwal S, Kunkel S, Mishina Y, Levi B (2020) Regulation of heterotopic ossification by monocytes in a mouse model of aberrant wound healing. Nature Communications 11: 722. DOI: 10.1038/s41467-019-14172-4.

Tőkési N, Kozák E, Fülöp K, Dedinszki D, Hegedűs N, Király B, Szigeti K, Ajtay K, Jakus Z, Zaworski J, Letavernier E, Pomozi V, Váradi A (2020) Pyrophosphate therapy prevents trauma-induced calcification in the mouse model of neurogenic heterotopic ossification. Journal of Cellular and Molecular Medicine 24: 11791-11799. DOI: 10.1111/jcmm.15793.

Torossian F, Guerton B, Anginot A, Alexander KA, Desterke C, Soave S, Tseng HW, Arouche N, Boutin L, Kulina I, Salga M, Jose B, Pettit AR, Clay D, Rochet N, Vlachos E, Genet G, Debaud C, Denormandie P, Genet F, Sims NA, Banzet S, Levesque JP, Lataillade JJ, Le Bousse-Kerdilès MC (2017) Macrophage-derived oncostatin M contributes to human and mouse neurogenic heterotopic ossifications. JCI Insight 2: e96034. DOI: 10.1172/jci.insight.96034.

Towler OW, Shore EM (2022) BMP signaling and skeletal development in fibrodysplasia ossificans progressiva (FOP). Developmental Dynamics: an Official Publication of the American Association of Anatomists 251: 164-177. DOI: 10.1002/dvdy.387.

Tseng HW, Kulina I, Girard D, Gueguen J, Vaquette C, Salga M, Fleming W, Jose B, Millard SM, Pettit AR, Schroder K, Thomas G, Wheeler L, Genêt F, Banzet S, Alexander KA, Lévesque JP (2022) Interleukin-1 Is Over-

expressed in Injured Muscles Following Spinal Cord Injury and Promotes Neurogenic Heterotopic Ossification. Journal of Bone and Mineral Research: the Official Journal of the American Society for Bone and Mineral Research 37: 531-546. DOI: 10.1002/jbmr.4482.

Urist MR (1965) Bone: formation by autoinduction. Science (New York, N.Y.) 150: 893-899. DOI: 10.1126/science.150.3698.893.

Urist MR, Lietze A, Mizutani H, Takagi K, Triffitt JT, Amstutz J, DeLange R, Termine J, Finerman GA (1982) A bovine low molecular weight bone morphogenetic protein (BMP) fraction. Clinical Orthopaedics and Related Research: 219-232.

Valverde-Franco G, Liu H, Davidson D, Chai S, Valderrama-Carvajal H, Goltzman D, Ornitz DM, Henderson JE (2004) Defective bone mineralization and osteopenia in young adult FGFR3-/- mice. Human Molecular Genetics 13: 271-284. DOI: 10.1093/hmg/ddh034.

van Kuijk AA, Geurts ACH, van Kuppevelt HJM (2002) Neurogenic heterotopic ossification in spinal cord injury. Spinal Cord 40: 313-326. DOI: 10.1038/sj.sc.3101309.

Villa-Bellosta R, Hamczyk MR, Andrés V (2016) Alternatively activated macrophages exhibit an anticalcifying activity dependent on extracellular ATP/pyrophosphate metabolism. American Journal of Physiology. Cell Physiology 310: C788-99. DOI: 10.1152/ajpcell.00370.2015.

Wang Y, Lu J, Liu Y (2022) Skeletal Muscle Regeneration in Cardiotoxin-Induced Muscle Injury Models. International Journal of Molecular Sciences 23: 13380. DOI: 10.3390/ijms232113380.

Weldon E, Razzouk J, Bohen D, Ramos O, Danisa O, Cheng W (2023) Medical Malpractice Litigation Due to Off-Label Use of Bone Morphogenetic Protein. Spine 48: 1575-1580. DOI: 10.1097/BRS.0000000000004563.

Yahara Y, Barrientos T, Tang YJ, Puviindran V, Nadesan P, Zhang H, Gibson JR, Gregory SG, Diao Y, Xiang Y, Qadri YJ, Souma T, Shinohara ML, Alman BA (2020) Erythromyeloid progenitors give rise to a population of osteoclasts that contribute to bone homeostasis and repair. Nature Cell Biology 22: 49-59. DOI: 10.1038/s41556-019-0437-8.

Yolcu YU, Wahood W, Goyal A, Alvi MA, Reeves RK, Qu W, Gerberi DJ, Goncalves S, Bydon M (2020) Factors Associated with Higher Rates of Heterotopic Ossification after Spinal Cord Injury: A Systematic Review and Meta-Analysis. Clinical Neurology and Neurosurgery 195: 105821. DOI: 10.1016/j.clineuro.2020.105821.

Yu PB, Deng DY, Lai CS, Hong CC, Cuny GD, Bouxsein ML, Hong DW, McManus PM, Katagiri T, Sachidanandan C, Kamiya N, Fukuda T, Mishina Y, Peterson RT, Bloch KD (2008) BMP type I receptor inhibition reduces heterotopic [corrected] ossification. Nature Medicine 14: 1363-1369. DOI: 10.1038/nm.1888.

Yuasa M, Mignemi NA, Nyman JS, Duvall CL, Schwartz HS, Okawa A, Yoshii T, Bhattacharjee G, Zhao C, Bible JE, Obremskey WT, Flick MJ, Degen JL, Barnett JV, Cates JMM, Schoenecker JG (2015) Fibrinolysis is essential for fracture repair and prevention of heterotopic ossification. The Journal of Clinical Investigation 125: 3117-3131. DOI: 10.1172/JCI80313.

Zhang D, Huang J, Sun X, Chen H, Huang S, Yang J, Du X, Tan Q, Luo F, Zhang R, Zhou S, Jiang W, Ni Z, Wang Z, Jin M, Xu M, Li F, Chen L, Liu M, Su N, Luo X, Yin L, Zhu Y, Feng JQ, Chen D, Qi H, Chen L, Xie Y (2021a) Targeting local lymphatics to ameliorate heterotopic ossification via FGFR3-BMPR1a pathway. Nature Communications 12: 4391. DOI: 10.1038/s41467-021-24643-2.

Zhang Z, Nam HK, Crouch S, Hatch NE (2021b) Tissue Nonspecific Alkaline Phosphatase Function in Bone and Muscle Progenitor Cells: Control of Mitochondrial Respiration and ATP Production. International Journal of Molecular Sciences 22: 1140. DOI: 10.3390/ijms22031140.

Editor's note: The Scientific Editor responsible for this paper was Sibylle Grad.